Journal of Applied Geophysics 219 (2023) 105217

Contents lists available at ScienceDirect

Journal of Applied Geophysics

journal homepage: www.elsevier.com/locate/jappgeo

Improved imaging of ground deformation and brine seepage around abandoned flooded salt mines by joint inversion of multiphysics data

Max A. Meju [a], Bernd Kulessa [b,c,*], Luis Gallardo [d], Sarah Thompson [c], Alastair Ruffell [e], Kieran Parker [f]

[a] Geomaxo Ltd, Lancaster, UK
[b] Swansea University, UK
[c] University of Tasmania, Australia
[d] CICESE, Mexico
[e] Queen's University Belfast, UK
[f] Geological Survey of Northern Ireland, UK

ARTICLE INFO

Keywords:
Hydrogeophysics
Joint inversion
Electrical resistivity
Seismic velocity
Ground instability
Groundwater contamination

ABSTRACT

Centuries of bad mine-flooding practice have left a legacy of underground salt mine collapse and contaminated discharges, the scale of which is only slowly being revealed now that ground processes have caused instability over decades to >100 years. Geophysical methods are used for mapping ground subsidence and groundwater contamination at such sites but suffer individually from non-uniqueness and with the underlying mechanism and processes not being well understood. Here, to reduce uncertainty and maximize accuracy we recover subsurface models with structural similarity enforced via crossgradients joint inversion of seismic refraction and dc resistivity data for the top 40 m at former mining areas in Carrickfergus region of Northern Ireland. The models in combination with multispectral image fusion, enable us to identify hitherto unknown mechanism of deformation and compositional changes consistent with the Chebotarev geochemical evolution of groundwater. We found evidence of concealed gravitational slump structures interpreted as being caused by water ingress weakening the gypsum-bearing marl bedrock (via gypsum dissolution and increased fluid pressures within marl) and leading to gravitational gliding deformation, expressed as curved subsidence bands and stepped thrusts coincident with surface zones of brine-mud seepage and sinkhole collapse. Our results have wide-ranging implications for best-practice assessment and management of abandoned flooded salt mines and the hazards they pose to ground stability and water resources world-wide.

1. Introduction

1.1. Problem definition

Abandoned mine workings often raise serious issues in relation to planning, development and environmental protection. Subsidence due to large scale salt mining and brine extraction is well documented in some areas of the UK and other parts of the world (Cooper, 2002; Bell et al., 2005; Kulessa et al., 2004; Carrier et al., 2022). The salt-mining region of Carrickfergus in County Antrim lies 15 km north-east of Belfast in Northern Ireland (see inset map in Fig. 1). The abandoned salt mines in this region are thought to pose a significant risk to public safety. In 1990 a programme of monitoring was initiated after the unexpected collapse of the Tennant mine in the area. The programme focused on six abandoned salt mines, of which Maiden Mount and French Park mines (Fig. 1) were considered to be of significant concern (Atkins, 2005). Both mines have caused considerable disruption to surface activities (e.g., road closure) and are thought to be central to the development of brine seepages in the early 2000s, degrading arable land near to the French Park mine as well as threatening encroaching infrastructure as the town of Carrickfergus is expanding uphill from Belfast Lough (Kulessa et al., 2004). The first surface brine seepage appeared at the south-west end of French Park in 2001 (**s1** in Fig. 2) shortly before the sinkhole collapse on 19 August 2001 in the Maiden Mount mine (CH in Fig. 2). Both mines are currently monitored by a number of techniques including changes in the water level in a number of boreholes and measurement of ground

* Corresponding author at: Swansea University, UK.
E-mail address: b.kulessa@swansea.ac.uk (B. Kulessa).

https://doi.org/10.1016/j.jappgeo.2023.105217
Received 11 March 2023; Received in revised form 15 September 2023; Accepted 20 October 2023
Available online 10 November 2023

movement in the immediate area (e.g., Cigna et al., 2017; Cooper, 2020). However, these techniques give little prior warning of ground collapse or subsidence and do not provide extensive information with regard to the subsurface structure, hydrogeology or presence and seepage of contaminants.

A major factor leading to instability of these mine workings was considered to be seepage of freshwater into abandoned mines via mine shafts and the engineered brining operations, resulting in the erosion of the mine pillars and roof strata and leading to a breakdown of the overlying strata and surface subsidence (Atkins, 2005; Arup et al., 1992). How to assure that this proposed mechanism of surface deformation is correct and how to remotely predict zones in the near-surface that are more likely to experience subsidence and/or seepage-related hazards still remain difficult propositions. As the Maiden Mount site is located uphill of French Park, it has been suggested that the hydraulic processes occurring at Maiden Mount may influence those at French Park. Moreover, there were significant mine spoil heaps on the surface and infiltrating water could generate saline leachate that can contaminate the near-surface, the extent of which is still unknown. The prospect of increased future rainfall and large flooding events in the northern hemisphere will exacerbate the problem even further. The Woodburn aqueduct ran across our study area (WA in Fig. 1) as a conduit below surface in pre-1935 ordnance survey maps (Sheet 52, 1930) as part of the main public water supply infrastructure for Belfast city. The location of the newer seep observed in our region in 2004 (s2 in Fig. 1) is geographically coincident with the trace of this aqueduct, but their possible connection is unknown.

While geophysical techniques are central tools for the non-invasive investigation of such abandoned flooded mine areas, individual methods on their own provide non-unique models of subsurface property and fluid-type present but integrating them together with good structural linkage maximizes accuracy, minimizes uncertainty and leads to a more reliable model, necessary for making cost-effective decisions to mitigate risks at such sites. This is what we set out to demonstrate in this paper, but the special focus is on identifying the attendant surface deformation mechanism necessary for understanding geohazards evolution and their mitigation for such sites. Using legacy multi-physics data acquired in 2004, we explore whether state-of-the-art joint inversion of seismic and electrical resistivity data, combined with electrical self-potential (SP) mapping, can provide valuable indications of possible land stability hazards (Kulessa et al., 2007; Thompson et al., 2012, 2017) and subsurface brine or leachate pools in the area of study (compared to individual resistivity and velocity models derived from using popular commercially available software and presented as supporting information *S1*). A quantitative integrated analysis of these multiphysics data will help to test the optimality of the past mapping of

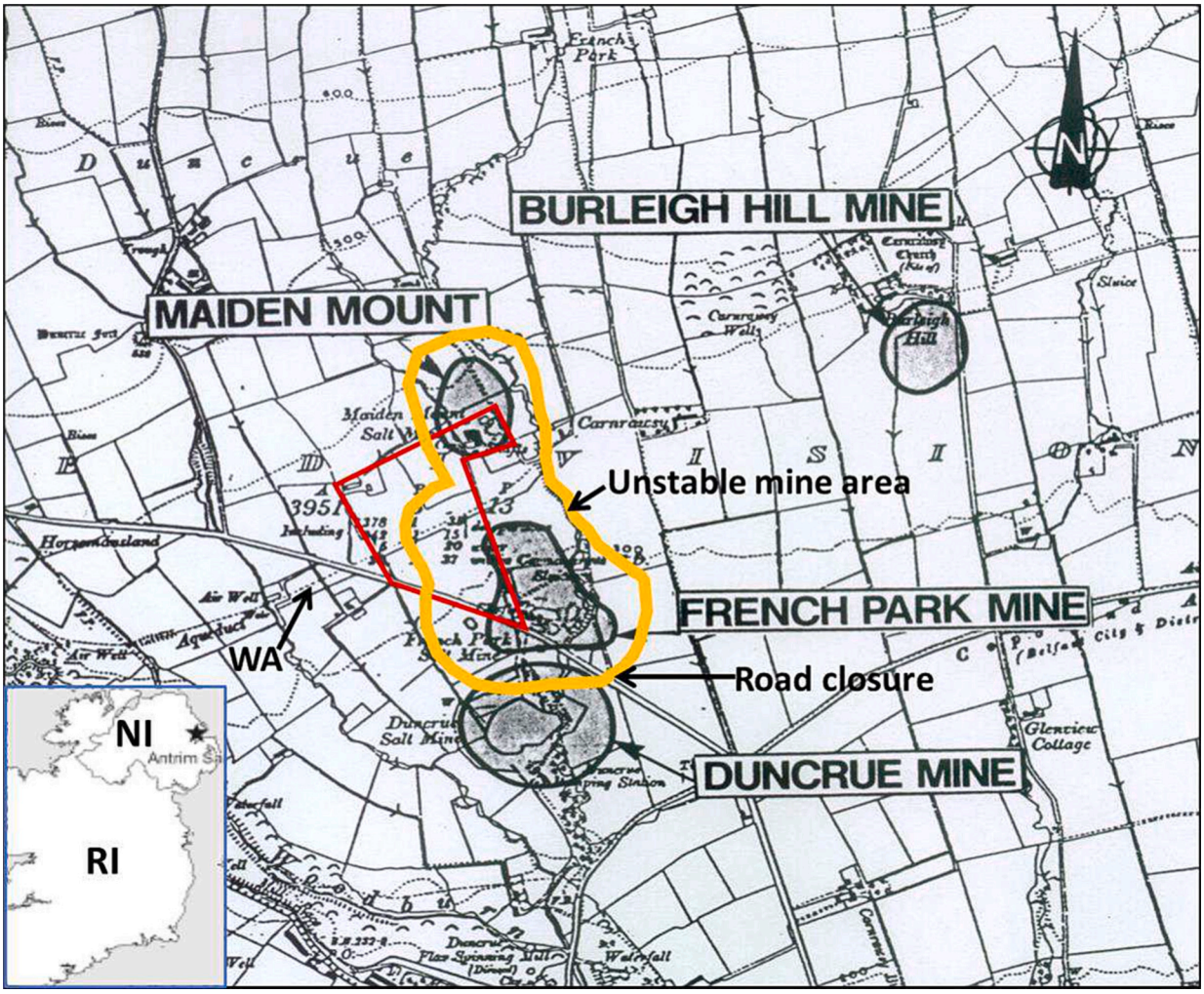

Fig. 1. Location and main features of our study area in Carrickfergus region of Northern Ireland. Shown is the ordnance survey map (adapted from Ordnance Survey Map of Northern Ireland, Sheet 52, 1930, 1:10560, reproduced with Crown copyright permission 2019) and the locations of Maiden Mount, French Park and Duncrue mines relative to our area of geophysical investigation (red polygon). Orange polygon shows the area classified as "unstable mine" in recent maps (e.g., Donald, 2015). Blue-rimmed inset map shows the location of our study area in Carrickfergus, County Antrim in Northern Ireland (NI); RI, Republic of Ireland; WA, Woodburn aqueduct. (For interpretation of the references to colour in this figure legend, the reader is referred to the web version of this article.)

hazardous mined area (Kulessa et al., 2004; Donald, 2015). It will also help us to better understand the deformation mechanism in the near-surface in response to underground space availability created by the past mining and brining operations as well as explain any related processes such as the possible hydraulic link between brine seepages in the south and subsequent sinkhole collapse in the north of our study area (features CH, s1 and s2 in Fig. 2).

1.2. Land use pattern at study site

The study site is underlain by Triassic rocks of the Mercia Mudstone Group (Griffith et al., 1983). It contains red marl with gypsum (Keuper Marl) in the upper 160–170 m above the halite deposits that were the target for Victorian brine-pumping extraction and are still mined to the north-east of the study area. Superficial deposits comprise of 5–25 m of glacial till with heterogeneous infill in places and maximum till thicknesses decreasing from about 20 m at Maiden Mount to about 15 m at French Park (Griffith et al., 1983; Nicholson, 2014). The extraction of salt in the Carrickfergus region (Fig. 1) began in the latter half of the 19th century when salt of the Mercia Mudstone group was discovered during coal exploration (Cooper, 2002). The French Park mine was sunk in 1870, after the neighbouring Duncrue mine was declared unsafe. Maiden Mount became operational around seven years later and was at the time the deepest mine in the UK. The dominant mining process in the area was the pillar and stall method, horizontal caverns supported by regularly spaced salt pillars (Cooper, 2002). In later years, flooding and uncontrolled brine extraction occurred in many of the mines for extended periods of time. This is likely to have dissolved some, if not all, of the supporting pillars, leaving the mines less stable and prone to collapse, increasing the likelihood of subsidence (Bell et al., 2005). Salt was extracted from the French Park Mine until around 1938 when the wall separating the mine from the adjacent Duncrue Mine collapsed, flooding French Park. Brining was initiated at this time and continued until the late 1950s.

A survey carried out in 1992 discovered that as a result of extensive brining, the mine cavity has over time, migrated towards the surface and all of the supporting pillars are thought to have collapsed (Arup et al., 1992). Due to this discovery, a nearby road was closed where it over-ran the southern end of the mine (see Fig. 1) and has since been re-routed, showing the effect of such historic mining has on infrastructure. Testing of borehole water samples showed that the salt concentration of the water in the mine was approaching saturation and it was suggested that this could halt further dissolution (Arup et al., 1992); however, the prevention of further dissolution depends primarily on the input of fresh water to the system, and a 2005 report concluded that mine collapse within the next 15–20 years is likely (Atkins, 2005).

Maiden Mount mine is located around 500 m to the north-west and upstream of French Park. The North and South shafts sunk in 1877 at the Maiden Mount mine were 900′ (274 m) and 913′ (278 m) deep respectively. Maiden Mount mine was taken over by Imperial Chemical Industries (ICI) in the 1950s and it was decided to change to brining (1953–1958) with the original shaft in-filled; two 900′ deep boreholes were sunk further north for this, one for flooding the mine caverns and the other for extracting brine. Maiden Mount and French Park mines eventually became connected due to brining operations at depth in later years (Cigna et al., 2017) and hence raising the possibility of major voids or galleries being present in the subsurface. On 19 August 2001, the Maiden Mount mine void space reached the surface and a water-filled cylindrical chimney (or crown hole) initially ~50 m wide and ~ 15 m deep opened up (Fig. 2) above a ~ 100 m wide, ~30–40 m deep void, some 100 m above the main salt-bearing horizon of Triassic mudstones (Kulessa et al., 2004). The collapsed area was fenced off and regularly

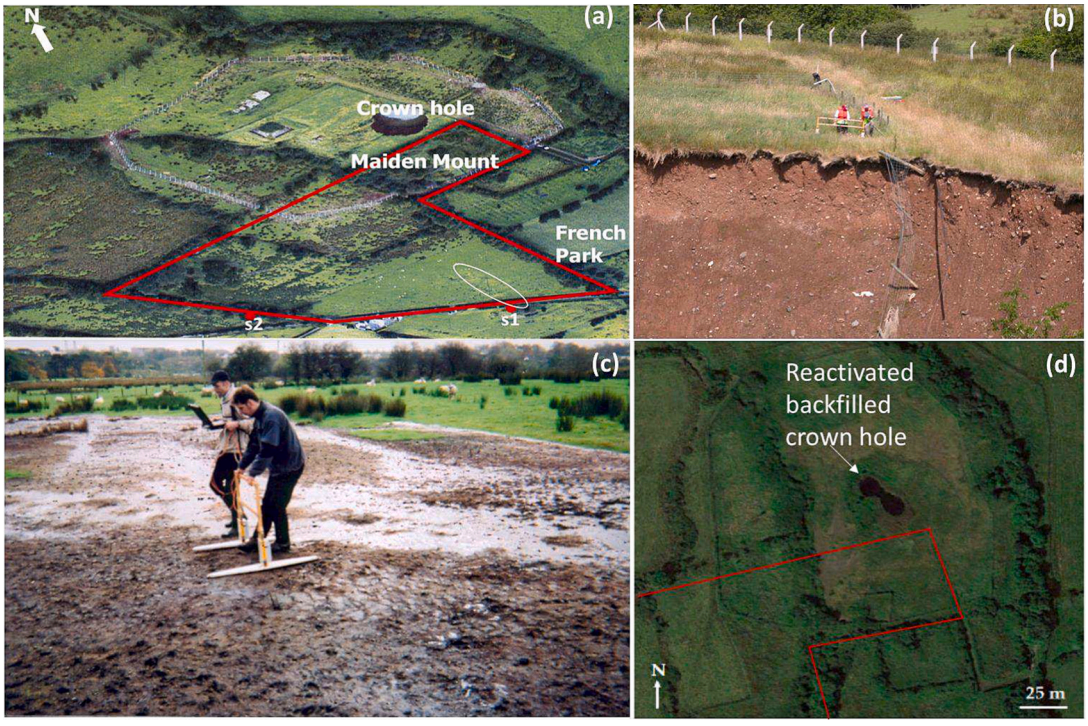

Fig. 2. Geological hazards at the site of the collocated multimodal geophysical surveys. (a) South-looking 2004 aerial photograph of the site showing the crown hole (CH), a collapse feature, of 19 August 2001 in Maiden Mount mine. Locations of surface brine seepages (s1 and s2) are shown by the red dots. The geophysical survey area is shown by the red polygon. White ellipse marks a localised topographic feature. ©Crown Copyright. (b) Segment of crown hole exposing thick drift deposit. (c) Photograph of surface brine leakage s1 ("old seep") that occurred in 2001 just before the crown hole and prompted the geophysical surveys described here with two ground radar operators for scale (Kulessa et al., 2004). s2 ("new seep") was observed in 2004. (d) Google Earth satellite image emphasising the reactivation of the backfilled area of crown collapse taken on 19 August 2016 (Cigna et al., 2017). (For interpretation of the references to colour in this figure legend, the reader is referred to the web version of this article.)

monitored while the possibility of in-filling the void and returning the land to agricultural use was being discussed (Atkins, 2005). Prior to any such remediation action, the stability of the land surrounding the crown collapse must be ascertained. Several geophysical measurements were made to support this quest (including the unpublished Multiphysics data adopted in the current study) and the collapsed area was subsequently backfilled (see Donald, 2015; Cigna et al., 2017; Cooper, 2020) but resulted in a much larger NW-SE trending surface depression (Fig. 2d) that altered the local topography (see Cigna et al., 2017, Fig. 8) suggesting that the underlying process remains poorly understood.

Maiden Mount and French Park mines are also thought to play a pivotal role in the development of a number of brine seepages in the area (Fig. 2), threatening its present-day agricultural value as well as encroaching infrastructure as the town of Carrickfergus is expanding uphill from Belfast Lough. The first seepage appeared at the south-west end of French Park in 2001, shortly before the Maiden Mount collapse. As the Maiden Mount site is located uphill of French Park, it has been suggested that the hydraulic processes occurring at Maiden Mount may influence those at French Park. Here, seepage through the former Marquis of Downshire mineshaft (MDM in Fig. 3) and along associated historic excavation surfaces was previously hypothesized to facilitate brine flow from depth to the ground surface based on GPR imaging (Kulessa et al., 2004). A simple pipe and hardcore drainage system was implemented with a herringbone design to capture water seepages over a large area (Atkins, 2005) but its effectiveness remained an open question. The surface brine leakage s1 ("old seep" in Fig. 2) that occurred in 2001 just before the crown hole collapse on 19 August 2001 in Maiden Mount mine prompted the 2004 multimodality geophysical surveys described below.

2. Methodology

2.1. Collocated multiphysics measurements

Electrical resistivity and seismic refraction depth sounding data were acquired along ten co-positioned survey profiles in 2004 to characterise

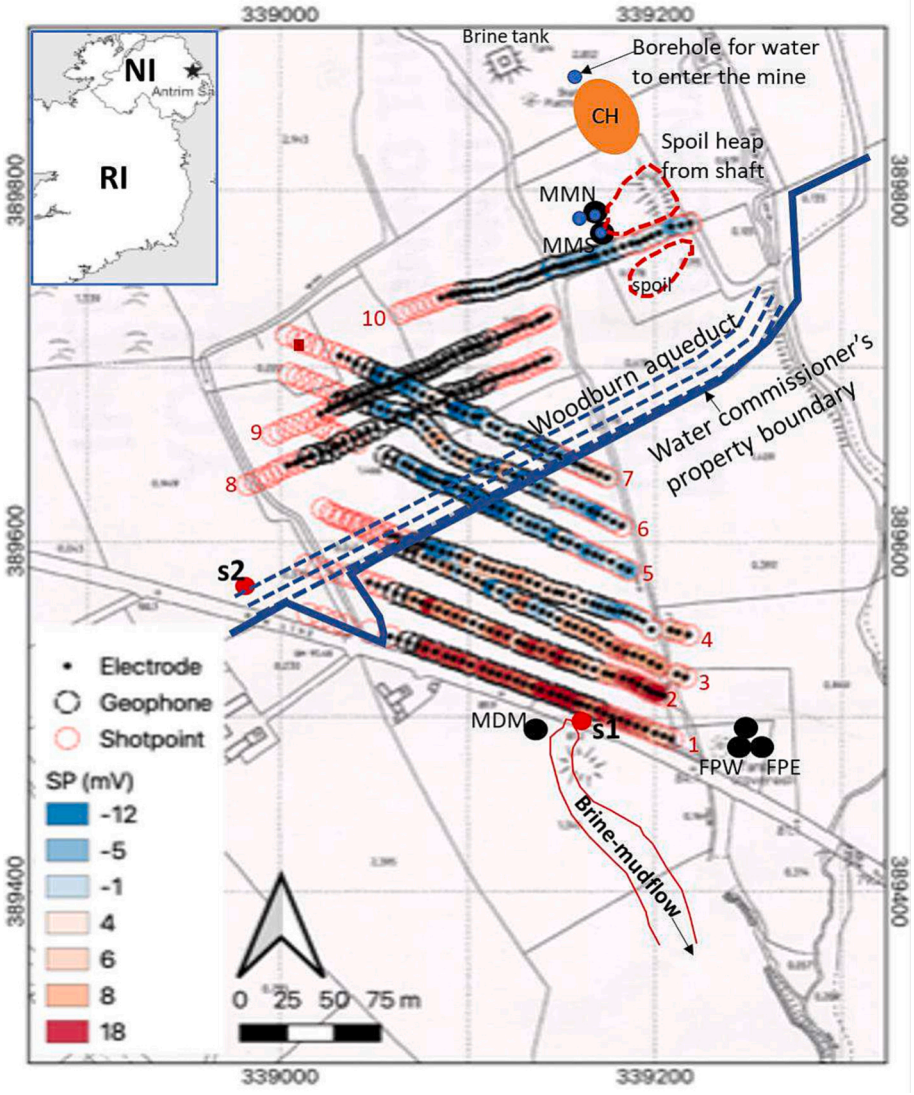

Fig. 3. Map showing the distribution of coincident dc resistivity, seismic refraction and SP measurement stations over an area of abandoned salt mines in Northern Ireland. Site cultural features and SP anomalies are shown on ordnance survey base map (Crown copyright 2002). SP anomalies in millivolts(mV) are colour-coded. The flow-path of the visible brine-mud seepage (**s1**) on farmland is shown by red polygon. MMN and MMS represent Maiden Mount North and South mineshafts. FPW and FPE are the French Park West and East mineshafts. MDM is Marquis of Downshire mineshaft. The ten survey line numbers are indicated in red. The trace of Woodburn aqueduct is shown by the 3 parallel dashed blue lines. The location of the fixed PMS 9000 reference electrode for the SP survey is shown by the dark red box at the northwestern end of line 7. Inset map shows our study site location in Carrickfergus area in County Antrim. NI, Northern Ireland; RI, Republic of Ireland. (For interpretation of the references to colour in this figure legend, the reader is referred to the web version of this article.)

the subsurface structure and detect and delineate any brine seepage from the upstream mine area of Maiden Mount towards French Park mine downstream (Fig. 1). The survey profiles were positioned to cover the agricultural area of interest between the two mines as comprehensively as possible within site access constraints, and each electrode or geophone position was measured in 3-D space using differential GPS. The electrical resistivity data were acquired using an *IRIS Sycal Pro* imaging system (Kulessa et al., 2007; Ruffell and Kulessa, 2009) with 36 stainless steel electrodes spaced at 5 m intervals along the survey profiles, so that each resistivity profile was 175 m long (Fig. 3). The Wenner-α electrode configuration was used because it provides the best compromise between vertical and horizontal resolution and signal to noise ratio (Sharma, 1997). For each electrode quadrupole between four and eight repeat measurements were acquired and stacked, with a desired maximum standard deviation of 3% between them. Seismic refraction data were acquired with a *Geometrics Geode* based system with 24 40-Hz geophones, a 12-lb sledgehammer and an aluminium plate (Kulessa et al., 2007; Hiemstra et al., 2011). The geophones were placed at the same positions as the stainless-steel electrodes used for our resistivity surveys, between profile distances of 15 m and 130 m, with respective forward and reverse off-end shots every five metres to profile distances of −30 m and 175 m. Data acquisition during periods of low surface wind speed, with a minimum of three stacks per shot location, ensured that high-quality seismic refraction data were acquired. Electrical self-potential (SP) data were subsequently acquired along eight survey profiles to identify whether any subsurface brine is stationary at present, or actively flowing down the presumed hydraulic gradient. The SP data were acquired manually with *PMS 9000* Pb-$PbCl_2$ lead-lead-chloride non-polarising electrodes (Petiau, 2000) connected by single-conductor wire to a METRA HIT 22S multimeter, having 10 MΩ input impedance (Doherty et al., 2010; Thompson et al., 2012). At each stainless-steel electrode position used in the resistivity surveys along lines 1–7 and 10, surface vegetation was removed (and then replaced) to ensure favourable ground contact. This facilitated the acquisition of high-quality SP data between a roving *PMS 9000* electrode placed sequentially in each cleared location, and a fixed *PMS 9000* reference electrode effectively buried in topsoil upstream of the survey area (Fig. 3). Standard closed-loop techniques of drift correction were used (Naudet et al., 2004; Doherty et al., 2010). The resulting processed SP data are presented in Fig. 3, showing a change in potentials possibly associated with seepage from uphill (north) to downhill (south) direction (Bolève et al., 2009; Thompson et al., 2012) where surface seepages are known to have occurred since 2001. The inferred seepage travel path is shown by the dashed white line in this figure.

2.2. Joint Inversion for common structure to maximize accuracy and reduce uncertainty

The cross-gradients joint inversion method originally developed for recovering structurally consistent models from electrical resistivity and seismic refraction data (Gallardo and Meju, 2003, 2004) will be adopted here. The structure-coupled inversion reconstructs those structurally similar images that match the measured electrical resistivity and seismic travel-time data as closely as possible, allowing for the fact that these data contain random noise whose distribution is Gaussian with zero mean and variance. Gallardo and Meju (2003, 2004) showed that joint inversion in this manner led to resistivity and velocity images with remarkable structural agreement, and as such were distinctly superior to those from more conventional separate 2-D inversions of the respective data sets (e.g., Meju et al., 2003), even in heterogeneous near-surface materials. By making the assumption that the different geophysical methods sample the same underlying geological structure (a common frame of reference), structural similarity is quantified and used to guide the joint inversion process. The linkage criterion is that the cross-products of the gradients of the dc resistivity property field and the seismic property field must be zero at a boundary. For a 2D profile oriented in the x direction with z direction pointing vertically downwards, if $\nabla \mathbf{m}_s(x,z)$ denotes the vector field of the gradients of the seismic velocity model and $\nabla \mathbf{m}_r(x,z)$ denotes that of dc resistivity model, then the cross-gradients function (Gallardo and Meju, 2002) is given by.

$$\boldsymbol{t}(x,z) = \nabla \mathbf{m}_r(x,z) \times \nabla \mathbf{m}_s(x,z) \tag{1}$$

and should tend zero at a significant structural boundary. The geological implication is that if a true boundary or transitional zone exists, it should be sensed by the resistivity and seismic models in the same or opposite direction. While this cross-gradients condition encourages structural conformity of the models, it also has some flexibility. First, the changes are not restricted in amplitude, which means that it allows each model to change according to their respective data requirements. Second, the condition does not force the models into a predefined common direction unless it is justified by the observed data; thus, the direction is determined by common agreement between the resistivity and seismic data sets. Finally, there is the possibility of allowing a boundary that only occurs in one of the models (resistivity or velocity) when either $\nabla \mathbf{m}_r(x,z)$ or $\nabla \mathbf{m}_s(x,z)$ vanishes somewhere in the model, which makes sense in cases where we have significant variation in only one of the physical property fields.

For joint dc resistivity and seismic refraction data inversion incorporating the cross-gradient constraint, the inverse problem is defined as (Gallardo and Meju, 2003):

$$min\left\{\Phi(\mathrm{m_r},\mathrm{m_s}) = \left\| \begin{matrix} d_r - & \mathrm{f_r}(\mathrm{m_r}) \\ d_s & \mathrm{f_s}(\mathrm{m_s}) \end{matrix} \right\|^2_{\mathrm{C_{dd}^{-1}}} + \left\| \begin{matrix} \alpha_r & \mathrm{Dm_r} \\ \alpha_s & \mathrm{Dm_s} \end{matrix} \right\|^2 + \left\| \begin{matrix} \mathrm{m_r} - & \mathrm{m_{Rr}} \\ \mathrm{m_s} & \mathrm{m_{Rs}} \end{matrix} \right\|^2_{\mathrm{C_{RR}^{-1}}} \right\} subject\ to\ t(\mathbf{m}_r, \mathbf{m}_s) = 0 \tag{2}$$

Here, $\boldsymbol{t}(\mathbf{m}_r,\mathbf{m}_s)$ represents the cross-gradients function, d_r and d_s represent the resistivity and seismic data respectively, $f_r(\mathbf{m}_r)$ and $f_s(\mathbf{m}_s)$ are respectively the dc resistivity and seismic traveltime data computed by forward theory, $\mathbf{C}_{dd}$ is the diagonal matrix of covariances of the data (which are assumed to be uncorrelated), $\mathbf{D}$ is the matrix of the smoothness operator, α_s and α_r are weighting factors that define the level of smoothness required in the models, $\mathbf{m}_{Rr}$ and $\mathbf{m}_{Rs}$ are the a priori model parameters with covariance $\mathbf{C}_{RR}$ (also assumed diagonal). The a priori model parameters and their covariance matrix are conveniently chosen to constrain the solution and reduce its variability for parts of the models not constrained by the data (for example areas not covered by seismic rays) and at the same time to limit the variability of the final models in zones where the certainty of the a priori model is high. Note that reliable a priori information can be incorporated into the objective function via the a priori model parameters and their covariance.

Indeed, follow-on applications and adaptations by others to a variety of geophysical data sets (e.g., Doetsch et al., 2010a, 2010b; Moorkamp et al., 2011, 2013; Um et al., 2014; Carrier et al., 2022) showed the cross-product given by eq. (1) to be remarkably robust in producing structurally-similar geophysical images. In the present case we can therefore expect to obtain images of structural anatomy of our study area, and any brine infiltration into it, that would be better than those

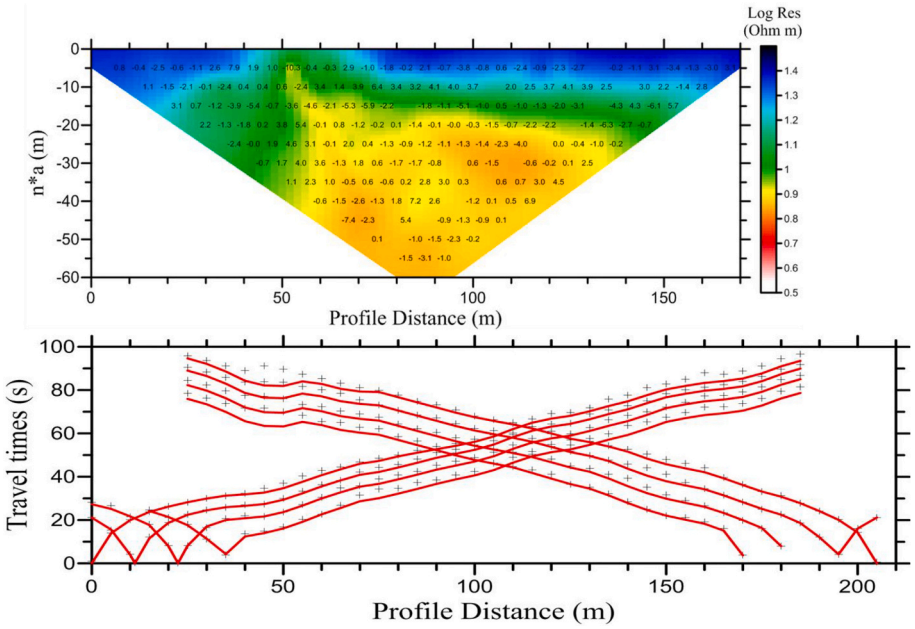

Fig. 4. Example of fit between observed and modelled Dc resistivity data (top image) and seismic first arrivals data (bottom plot) for Line 2 for the crossgradient resistivity and velocity models shown in Fig. 5. In the top plot, the coloured image is a pseudo-depth section of the observed dc apparent resistivities in logarithmic scale and the annotated values are the inversion residuals (i.e., differences between observed and modelled data) in %. The successively increasing measurement array length n*a is given by the fixed dipole electrode spacing of a = 5 m times a multiplicative number n. In the bottom plot, the plus symbol represents observed travel-time data and the red solid lines are the model responses at the various geophone stations making up the refraction array. (For interpretation of the references to colour in this figure legend, the reader is referred to the web version of this article.)

obtained by separate inversion of our seismic refraction and electrical resistivity data. The interested reader is referred to these earlier publications and reviews by (Gallardo and Meju, 2011) and (Meju and Gallardo, 2016) for exhaustive details of this structure-coupled joint inversion scheme now widely used for quantitative integration of Multiphysics measurements. We jointly inverted all the seismic and resistivity datasets to yield models that are structurally consistent and fit the observed data best in a statistical sense (normalised RMS error of 1) as in the representative example for line 2 shown in Fig. 4. The finite-difference based computations employed a common numerical grid for the joint inversion process but with separate dc and seismic forward calculation grids optimally matched to the sensitivity requirements of each method (Gallardo and Meju, 2003, 2004). The results for all the ten survey lines are consequently presented from east to west following the seismic profiling direction adopted in our common grid joint inversion scheme.

2.3. *Integrated electro-mechanical systems appraisal to improve decision making*

We appraise the reconstructed physical models along each survey line pixel-by-pixel for resistivity-velocity relationships or diagnostic patterns presented as a cross-plot (Gallardo and Meju, 2003, 2004; Meju et al., 2003) which is popular for reservoir characterization in the environmental and petroleum industries (Meju et al., 2003; Doetsch et al., 2010a; Moorkamp et al., 2013). For post-inversion extraction of robust features of these models, we adopt the geospectral imaging (RGB blending) approach (Gallardo et al., 2012). We blend RGB images of the resistivity and velocity models into the cross-plot for more robust trend deductions. For insights on the possible presence of subsoil contaminant plumes, material flow or cavities, we search for consistent patterns in the SP profiles and these resistivity-velocity images of the subsurface and their correlation with any features visible on the ground surface (brine seepages or mine waste spoils mapped in Fig. 1). To avoid over-interpretation of the joint inversion models, we examine the seismic ray-paths and only the features crossed by sufficient ray paths are deemed to be justified by the field data thus enabling us to define the effective zone of investigation (EZI) from joint inversion.

For illustration, the resulting joint inversion models for line 2 are shown in Fig. 5. Note the remarkable structural similarity of the main features present in the reconstructed models (Fig. 5b and c). The geospectral image is also shown in Fig. 5d to guide the interpretation of the subsurface. The seismic ray-paths are shown superimposed on the geospectral image for comparison; only those features crossed by sufficient ray paths are deemed justified by the field data and hence the yellow line in this image is our interpreted limit of the zone of effective investigation. We also computed a resistivity-velocity cross plot from the joint inversion models, shown on the righthand-side of the geospectral image in Fig. 5d. The cross-plot enables the distinction between unconsolidated sediments and consolidated rocks or local basement as well as the pattern of fluid saturation (e.g., Gallardo and Meju, 2003; Meju et al., 2003) and relative direction of changes in total dissolved solids (TDS) or saltiness of the fluid saturating a given material (see red arrow in this cross-plot). In general, the geographical coincidence of low velocity and high resistivity (LVHR) could signify the presence of unsaturated non-confined loose materials, freshwater or voids; low velocity and low resistivity (LVLR) could signify confined brine-mud pools; and high velocity and moderate resistivity (HVMR) could signify consolidated marl with gypsum as annotated in Fig. 5b, c and d. The collocated SP data (Fig. 5a) enable us to further distinguish between competing scenarios in our integrated approach; low SP values would corroborate our inferred positions of unstable ground or material transport. We have rigorously applied the above workflow to get the interpretable results for the ten survey lines (summarised in Fig. 6 and supplementary material S1).

3. Results and their geological appraisal

3.1. *Structurally-consistent subsoil models*

The reconstructed distributions of electrical resistivity and seismic compressional wave velocity (Vp) along two survey lines selected for illustration are shown in Fig. 6 together with their associated

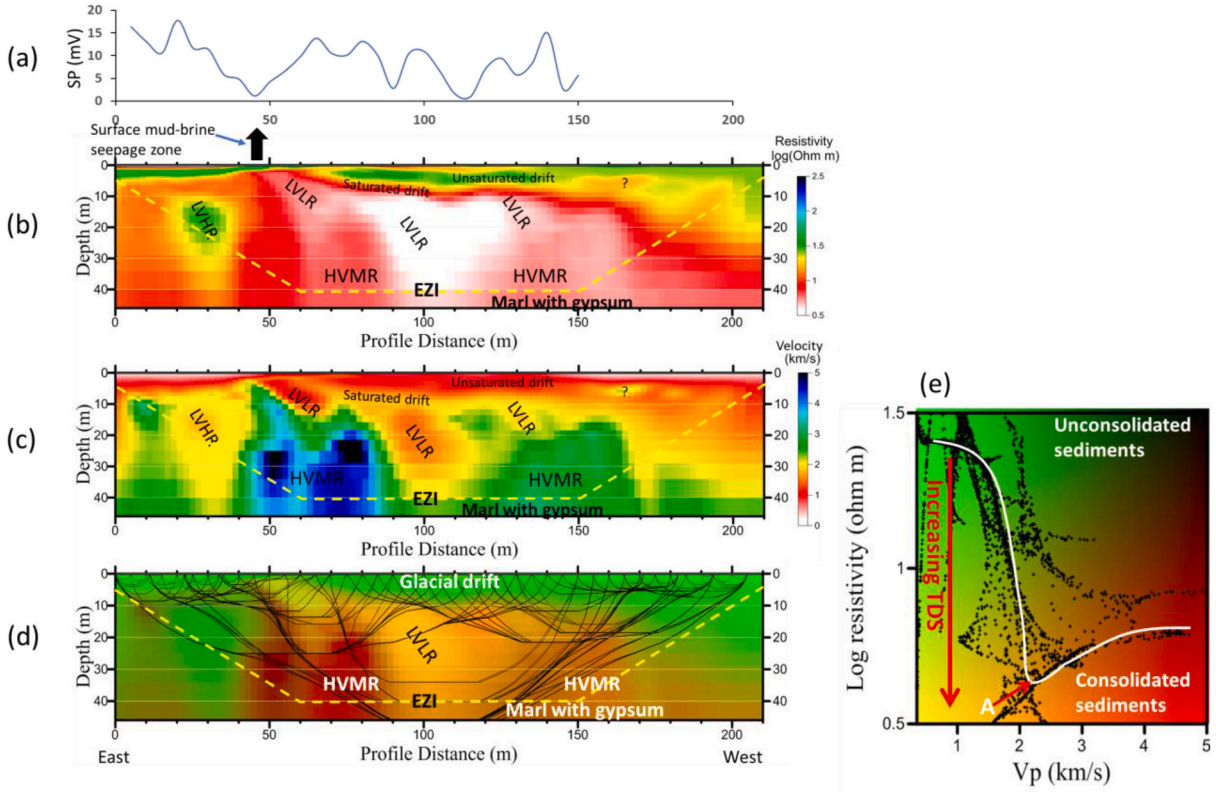

Fig. 5. Example of resulting integrated structurally consistent models from crossgradient joint inversion and geospectral imaging of Dc resistivity and seismic first arrivals data compared with SP profile for Line 2. (a) SP profile, (b) resistivity model, (c) seismic compressional velocity Vp model, (d) geospectral image from RGB blending of resistivity and velocity models, and (e) cross-plots using data from b, c and d. The black bold arrow in (b) marks the position of mud-brine seepage on the surface. HVMR, high velocity-moderate resistivity. LVLR, low velocity-low resistivity. LVHR, low velocity-high resistivity. The seismic ray-paths are shown in (d) and only those features crossed by sufficient ray paths will be deemed justified by the field data. The yellow line in the images is consequently our interpreted limit of the effective zone of investigation (EZI) from joint inversion. In (e) is an interpretative geospectral and resistivity-velocity cross-plot where the point A marks the boundary between unconsolidated sediments and consolidated sediments or local water table; TDS, total dissolved solids. (For interpretation of the references to colour in this figure legend, the reader is referred to the web version of this article.)

geospectral image and resistivity-velocity cross-plot. (The results for all the ten lines are summarised in the supplementary material *S1*.) All the lines are presented from east to west following the seismic profiling direction used for the common numerical inversion grid. The computed responses for all the inversion models matched the observed seismic travel time and apparent resistivity data to within a normalised root-mean square (nRMS) error of 1 as in the example shown for line 2 in Fig. 4. In Fig. 6 *(and S1)*, notice the remarkable structural consistency between the seismic velocity and Dc resistivity models for each line as expected for cross-gradient imaging. The glacial till and marl with gypsum in the top 40 m shows up well in these structurally consistent images. In most cases, the glacial cover is divisible into upper and bottom sections of different resistivities and velocities, suggesting different levels of fluid saturation (Figs. 5 and 6). Interestingly, the subsurface resistivity and velocity pattern in the un-mined northwest segment of our study area is different from that in the mined segments. Notably on line 10, there is a marked change in the glacial till layer resistivity between the low-resistivity eastern half passing over the spoil heap from the main shaft at Maiden Mount mine and the western half which is of much higher resistivity (Fig. 6). This could suggest that there is a significant contribution to this lowering of resistivity from leaching of mine tailings dumped at the ground surface by infiltrating water.

In terms of subsurface structure, the dominant low-resistivity (i.e., electrically conductive) zone in the study area can be used as a marker for event correlation purposes. In our joint inversion models, the top and bottom of this conductive (fluid saturated) zone is not smooth going eastward towards mined land as exemplified by Lines 1 and 10 shown in Fig. 6. Its base is the top of the consolidated marl with gypsum layer which appears to be characterised by parallel bands of steep zones of relatively high velocity (2.45- $>$ 3.1 km/s) and moderate resistivity ($>$20 Ωm) bordered by low-resistivity and low-velocity bands, consistent with the HVMR features imaged on Line 2 in Fig. 5. There is remarkable regularity in the HVMR distribution from north to south (Figs. 5, 6 and *S1*) which may well be an indication of past ground movement or mass transport of mobile materials from below and hence constitute subsidence hazards. Dry salt would cause such high seismic velocities but is unlikely to exist at these shallow depths in the damp climate of Northern Ireland; marl with gypsum was encountered in mine shafts at that depth and the typical Vp values for marl rocks are higher than 2.8 km/s (Mari et al., 1999). Understanding the full implication of the evinced structural geometry for the attendant subsurface processes will be explored later, noting that brine-mud spillage is visible on the surface on line 1 where the 5 m thick cover of unsaturated deposit is breached by this conductive marker unit (Fig. 6).

3.2. *Integrated analysis of inferred water-rock interface properties*

In terms of the attendant hydrodynamic processes, the resistivity-velocity cross-plots and spectral signatures extracted from our joint inversion models can provide useful insights (and are presented for all ten lines in Figs. 6 and *S1*). The geospectral images and crossplots for Lines 1 to 4 are similar and show the unsaturated part of the glacial till to be characterised by high resistivity (ρ) and low compressional wave velocity Vp ($<$1 km/s) while the saturated till and/or uppermost part of the clay with gypsum layer is marked by low resistivity and increasing Vp (Figs. 6 and *S1*). Beneath them is a zone consisting of consolidated

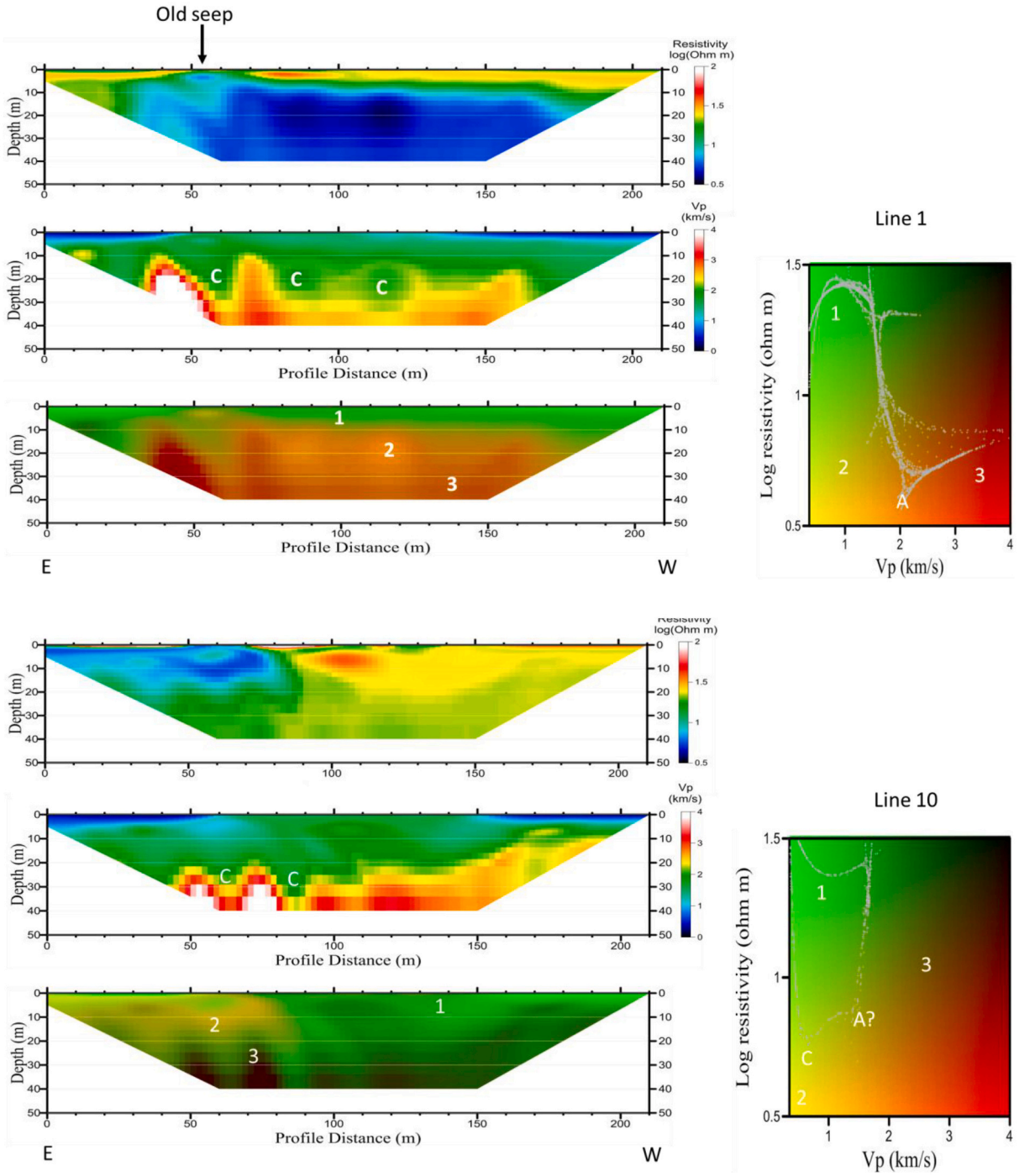

Fig. 6. Representative examples of the result of 2D cross-gradient joint resistivity-velocity inversion and geospectral imaging for lines 1 and 10 where surface brine-mud seepage or subsidence occurred. For each line are shown the resistivity (top left), velocity (middle left) and RGB blended geospectral (bottom left) models; the associated interpretative resistivity-velocity cross-plot is shown in the right top corner. The numbers 1, 2 and 3 refer to lithologic or hydrologic facies (or clusters) with their boundary points represented as A or B. Symbol C in the velocity models are zones of significant irregularity that possibly suggest ground instability. The black arrow marks the location where brine spilled onto the ground surface on line 1 (old seep s1) and its inferred position on line 2.

marl with gypsum marked by resistivity and velocity increasing with depth. The diagnostic boundary between the unsaturated and saturated zones is labelled point A (Fig. 6). For lines 1 to 4, point A is characterised by Vp of 1.8–2.1 km/s and log ρ of 0.5–0.7 Ωm suggesting the possible presence of brine (a Vp of ~1.5 km/s will be expected for freshwater-saturated sediments (Gallardo and Meju, 2003; Meju et al., 2003). However, for lines 5 to 8 (Fig. *S1*), there is a superposition of two resistivity-velocity trends with significant resistivity reversal at points A (Vp = ~2 km/s; log ρ = 0.65–1.1 Ωm) and B (Vp = 2.7–3.1 km/s; log ρ = 1.2 Ωm) with B being consistent with the typical Vp value of marl rocks (Mari et al., 1999). Incidentally, these are the survey lines that extend from the westerly unmined areas to the easterly mined areas with spoil heaps on the surface lending credence to our inference (discussed later) of potential infiltrating freshwater in the western part and leachate brine in the eastern part. Furthermore, it was noted that the parameters of point A are similar for all the line segments located within the mined areas (see Figs. 6 and *S1*). The lowest resistivity at point A is seen on line 4 while the highest value is found upstream on line 9 (with A

parameters of Vp = 2.35 km/s, log ρ = 1.2–1.25 Ωm) and the western part of line 8 (with A parameters of Vp = 1 km/s, log ρ = 1.4 Ωm). This is consistent with our inference of upstream partitioning of infiltrating water-types and could suggest a genetic link between north and south in which the groundwater's composition is evolving following the classic Chebotarev (1955) sequence (discussed in more detail below). It doing so, composition changes from relatively low TDS (synonymous with higher resistivity) in upstream northerly recharge area through Line 4 in the middle part where it is slowly moving or relatively stagnant (with lowest resistivity or highest TDS) to the southerly discharge area near Lines 1 and 2.

3.3. Appraisal of different results at known hazardous locations

Seismic velocity imaging is known to help resolve structure while resistivity imaging identifies significant brine-filled materials or cavities in the subsurface. It is well-known that a multiphysics approach combining both methods using the cross-gradients algorithm leads to better models than possible from the individual methods (Gallardo and Meju, 2003, 2004). Line 1 crossed the zone of surface brine seepage in the east while Line 10 extended eastwards into the area of known collapse structures. Also, both lines cut across areas of known surface spoil heaps from mining according to historical ordnance survey maps.

In Fig. 7, we compare SP profiles, our models from cross-gradient joint inversion and those from separate inversion using other well-established software. In this figure can be seen features that were reliably sensed by electrical resistivity imaging but not satisfactorily by seismic velocity imaging on its own (white stars) and those imaged by seismic data but not reliably sensed by resistivity inversion on its own (black arrows) using the conventional separate inversion software. Notice that both sets of features were completely recovered and refined in the cross-gradients joint inversion resistivity and velocity models including the surface breakthrough or isolated feature at the sites of surface spillage or sinkhole collapse (black star). For example, along line 1 the individual seismic tomographic inversion (Fig. 7e) identifies a steep dyke-like feature at profile distance 40–70 m and minor doming of the boundary of the consolidated marl with gypsum layer at profile distance 145–160 m. A steep feature is imaged at the 40–70 m profile location but not the dome by the individual resistivity imaging (Fig. 7d) and the depth to its top as well as the lateral extents are different. The joint resistivity-velocity inversion models (Fig. 7b and c) consistently show two steep features at the 40–70 and 145–160 m profile distances. There are also two localised conductive bodies of circular cross-section seen only in the individual resistivity and joint resistivity-velocity models but not imaged by separate seismic inversion. The seismic velocity model from joint inversion benefited from the contribution from resistivity imaging and vice versa in the cross-gradients process. The SP anomaly along this line is relatively higher over the zone of steep HVMR feature than elsewhere but with depressed values at the location of known surface brine-mud spillage.

Further upstream along line 10, the individual resistivity inversion model shows a corrugated low resistivity layer in an otherwise relatively resistive half-space and confined to the eastern half of the transect (Fig. 7d). This is captured in the joint seismic-resistivity inversion models but not in the individual seismic Vp model (Fig. 7e). This electrically conductive feature is deepest where the SP anomalies are most strongly negative in magnitude. The joint inversion models (Fig. 7b and c) showed that the western half is clearly different from the eastern half above the basal marl with gypsum layer of corrugated topography. The shape of the boundary of the consolidated marl with gypsum layer is surprisingly similar to that seen on Line 1 in our joint inversion models. This is significant and suggests a link between the sinkhole collapse in the north and the brine-mudflow (exit stream) in the south.

4. Discussion

A major factor leading to instability of these mine workings was considered to be seepage of freshwater into abandoned mines via mine shafts and the engineered brining operations, resulting in the erosion of the mine pillars and roof strata and leading to a breakdown of the

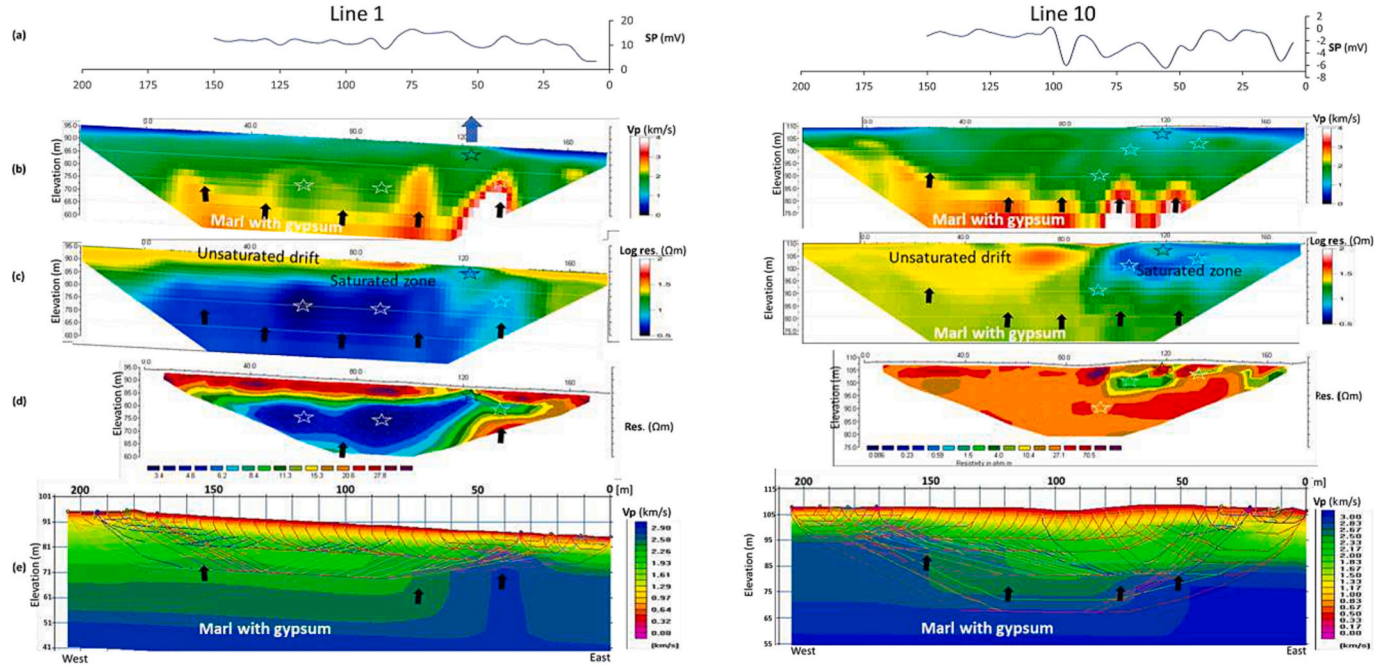

Fig. 7. Comparison of various geophysical results along two key lines where surface brine-mud seepage or subsidence occurred. (a) SP profile; (b & c) crossgradients velocity and resistivity models; (d) separate dc resistivity inversion using the commercial package Res2Dinv; (e) tomographic inversion of seismic refraction data using SeisImager commercial software. The blue arrow marks the location where brine spilled onto the ground surface on line 1 (see Fig. 2c). Black arrows and white stars are positions of features used for assessing the similarity or dissimilarity of the reconstructed images of the subsurface. (For interpretation of the references to colour in this figure legend, the reader is referred to the web version of this article.)

overlying strata and surface subsidence. The prospect of increased future rainfall and large flooding events in the northern hemisphere will exacerbate the problem even further. On ordnance survey maps of UK of pre-1935 is found the (Belfast City & District Water Works) Woodburn aqueduct running across our study area (see Figs. 1 and 3) and was previously part of the main public water supply infrastructure for Belfast city. Shown as a dotted line on the map until 1935, it presumably was mostly, if not entirely, closed (i.e., a tunnel/conduit/pipe below surface) and there were air wells built into it at intervals along the whole length of its track (WA in Fig. 1) from Monkstown right through to Carr's Glen Reservoir and Belfast Waterworks in Northern Ireland. Such a water-supply infrastructure may have left relict geophysical footprints and it will be instructive to distinguish them from those of any leachate pools emanating from mine spoil heaps on the ground surface.

The SP, seismic velocity and resistivity profiles for lines 5, 6 and 7 which cross the original position of this aqueduct are summarised in Fig. 8. It would appear at first glance that the Woodburn aqueduct-related facility (also reported as the Water Commissioner's French Park conduit in old mine surveyor's maps) was a potential contributor of water (leakage or natural recharge?) to the subsoil since there is a somewhat consistent change in the resistivity structure at depth across that locality on lines 5, 6 and 7. This can be deduced along a zone offset ~10 m to the southeast (downhill) of the main axis of the aqueduct in Fig. 8 and coincident with the eastern boundary of the water conduit facility where ditches were apparent on old maps. However, notice the corrugated nature of the cover layer on line 7. The cover layer becomes progressively more corrugated eastward on line 10 (see Fig. 6). Corrugated low resistivity and enhanced velocity features are found both up-dip and down-dip of the known hydraulic gradient in our study area, which may not be adequately explained by leakage from the Woodburn aqueduct. What is the attendant deformation mechanism at play here?

4.1. *Inferred water-associated ground deformation mechanism and attendant processes*

The joint inversion sections and coincident colour-coded SP anomalies are presented at their respective geographical positions in Fig. 9 to permit an areal assessment of the results. The known extents of underground mining from past historical records and the zone of visible brine spillage are also shown in this figure for reference. The low resistivity zone on lines 1 to 7 extend from the west to the north-south running surface depression at the eastern edge of survey lines 1–7 while that on line 10 extends from the east towards this surface depression (see Fig. 2a). The low resistivity zone is shallowest towards the area of known underground mining to the east and also underneath the area shown on the map to contain mine spoil heaps; this observation would suggest rainfall and/or surface water infiltration and leaching of mining waste as the possible sources (yellow and blue arrows in Fig. 9) of the laterally-confined conductive anomaly. It is obvious in this figure that the conductive anomaly extends westward beyond the currently accepted limit of unstable mined ground (Donald, 2015).

When considered in the context of the SP anomaly map (Fig. 3), the resistivity images could at first glance be taken to suggest the evolution of a low-resistivity brine plume from upstream (line 7 or even line 10) to downstream (Line 1) such that, especially in Lines 1 and 2, there evolves a connection between the plume and the ground surface where surface brine-mud leakage occurred in a farmer's field (Fig. 2c). Earlier study (Kulessa et al., 2004) interpreted this connection as a former mineshaft based on GPR data. However, does this simplistic analysis explain all our observations at this site? The resistivity-velocity models show distinct shallowing depth-wise of steep thrust-like structures in the localised area with marked positive SP values on lines 1 to 3 (Fig. 3). However, Figs. 5 and 7 also show that the SP profile across the area of surface brine-mud seepage has a local negative signature superimposed on the areal positive anomalies. Some other mechanism may be at work in the subsurface in this area where the mined and un-mined areas evidently have contrasting velocity and resistivity characteristics.

Based on the similar subsurface structure derived from data inversion, we opine that the resistivity and velocity models evoke a picture consistent with concealed gravitational gliding deformation or land sliding (Fig. 10). Water ingress (from rainfall, surface ponds and widespread artificial injections; Fig. 9) would have facilitated gypsum dissolution creating enhanced permeability and increased fluid pressures within the otherwise impermeable host marl, significantly weakening its load bearing capacity and leading eventually to gravitational gliding deformation now expressed as curved subsidence bands and stepped toe-thrusts coincident with surface zones of brine-mud seepage and sinkhole collapse. The role of water in the formation of landslides as well as thrust structures in front of coastal

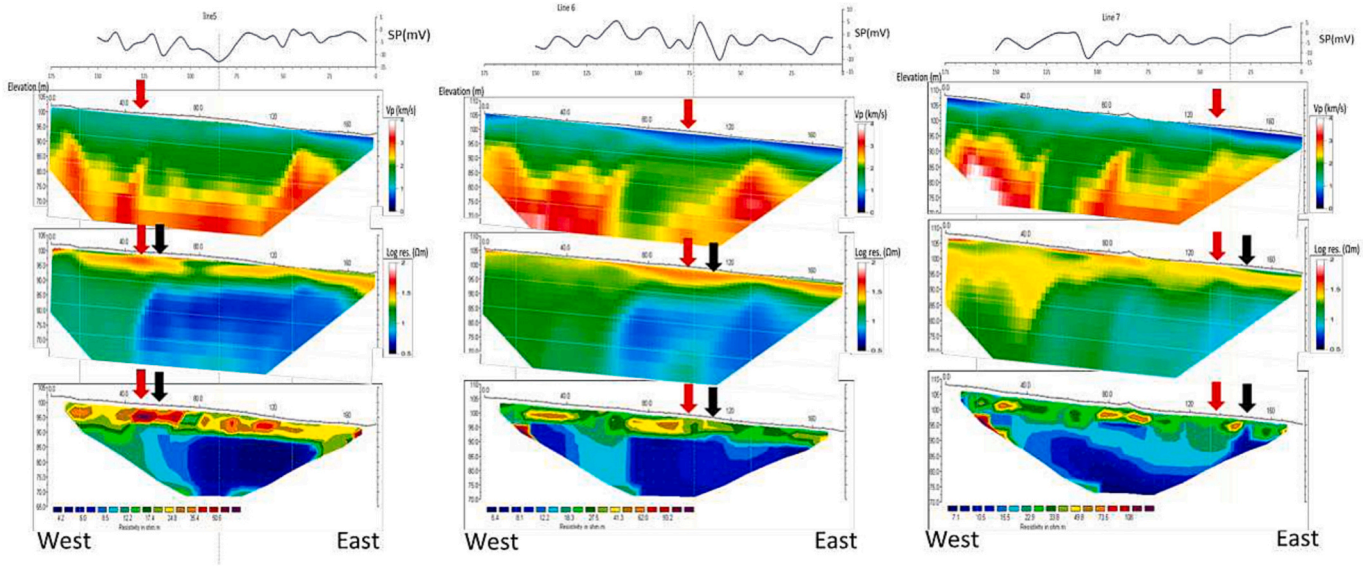

Fig. 8. Correlation of coincidentally-located SP profile, cross-gradients velocity and resistivity models, and independently obtained Res2Dinv resistivity models for lines 5, 6 and 7 crossing the Woodburn Aqueduct (or Water Commissioner's French Park Conduit) previously used for water supply to Belfast city (see Figs. 1 and 3) whose approximate location is indicated here by the downward-pointing red arrow. Black arrow is the location where each survey line crossed the eastern property boundary of the Water Commissioner parallel to the axis of the aqueduct and probably served as a downhill recharge zone. (For interpretation of the references to colour in this figure legend, the reader is referred to the web version of this article.)

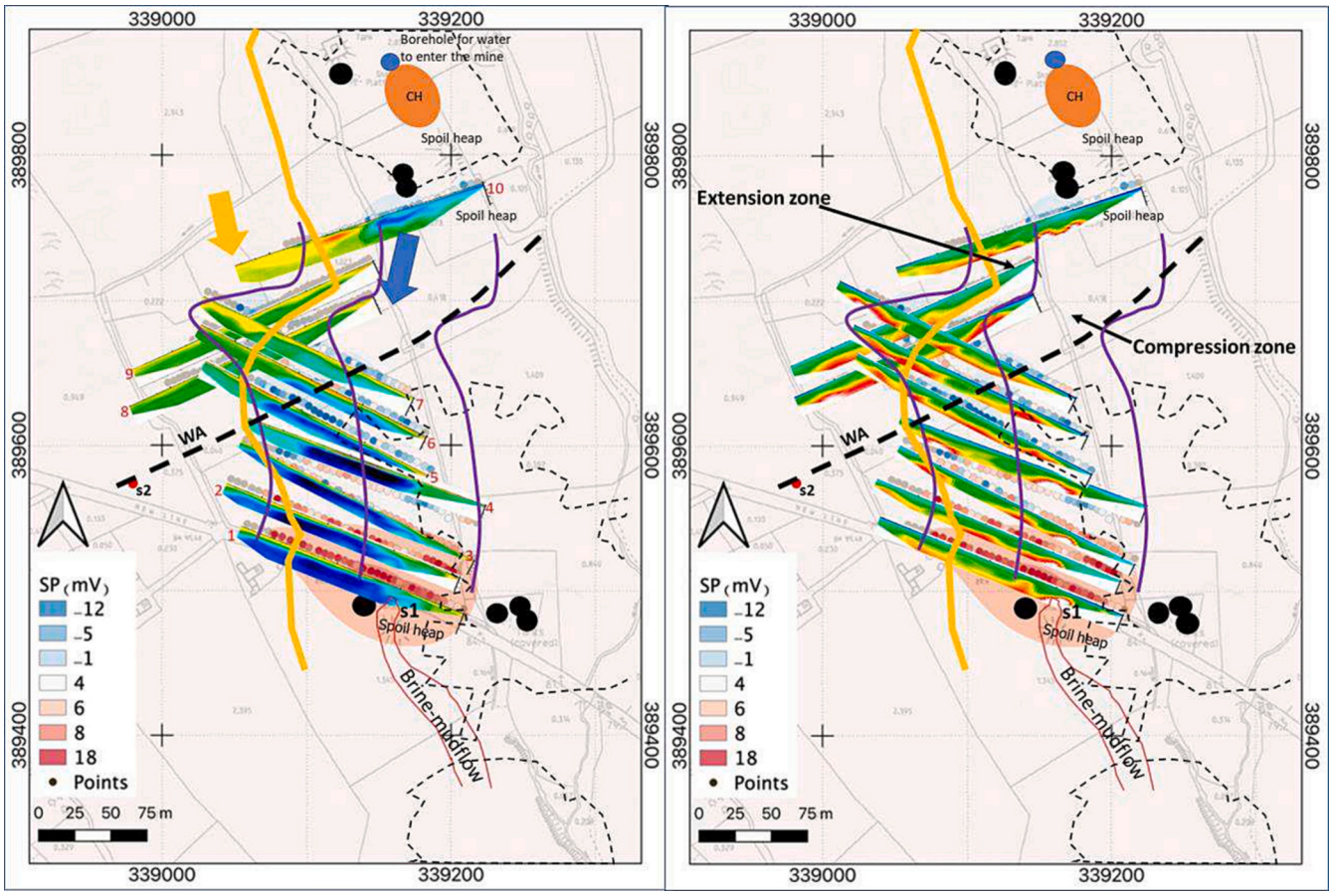

Fig. 9. Interpreted evidence of partitioned (extensional and contractional) ground deformation and groundwater compositional changes from north to south. Shown are fence diagrams of cross-gradients resistivity sections (left) and velocity sections (right) for lines 1–10 and known site hazards with colour-coded SP anomalies in the background. The black dashed lines indicate the known extent of underground mining from ordnance survey maps of Northern Ireland. Recent interpretation of extent of unsafe mined land is shown by the thick orange line (adapted from Donald, 2015). Purple lines demarcate the bands of extensional and contractual deformation while the wide arrows show our interpreted trend of geochemical evolution of groundwater (Chebotarev, 1955) from the northerly recharge area (orange – freshwater; blue – includes leachate from spoil heap) to the southerly discharge zones **s**1 and **s**2. (For interpretation of the references to colour in this figure legend, the reader is referred to the web version of this article.)

landslides is well-known (e.g., Knight, 2005). Trude et al. (2012) invoke local mobilization, diapirism, allochthonous flow, withdrawal and welding of salt to explain the collapse structures and fold-thrusts observed in the Mercia Mudstone Group on the Bristol Channel coast in Somerset, UK. It is also well-known for originally marine deposited clays with a pronounced salt content (quick-clays) that, if leached by freshwater, lose their strength and may lead to land sliding (Krawczyk and Polom, 2018). An analogous behaviour is apparent in failed dam foundations made up of gypsum-bearing clays (e.g., Aghajani, 2018). Here, gravity gliding led to the formation of what looks like toe-thrusts (imbricating thrusting) in the resistivity and seismic images (Figs. 9 and 10). The area of corrugated till-marl interface to the east would correspond to toe-thrusts while the steep truncations to the west would correspond to normal faults (Fig. 10a and b) as documented in gravity gliding in different environmental settings (e.g., Knight, 2005; Trude et al., 2012; Misra, 2018; Aghajani, 2018).

For event timing, it is significant that our results suggest a genetic link between north and south (Fig. 9) in which the groundwater's composition is evolving following the classic Chebotarev (1955) sequence. That is, composition changes from relatively low TDS (synonymous with higher resistivity) in upstream northerly recharge area through Line 4 in the middle part where it is slowly moving or relatively stagnant (with lowest resistivity or highest TDS) to the southerly discharge area near Lines 1 and 2. The corrugated structure of the saturated zone in the east suggests that the groundwater compositional changes (requiring long residence time) preceded the gravity-driving deformation. We surmise that the seepage **s**1 and crown hole collapse CH are related events; this sinkhole collapsed to a depth of ~15 m consistent with the conductive corrugated feature on line 10. It is possibly related to the crestal collapse of a toe-thrust system. The newer seep **s**2, geographically coincident with the trace of the old Woodburn aqueduct, may thus be due to this gravity-driven lateral flow possibly exploiting the pre-existing subsurface conduit.

Our new inference of the water-rock-gravity interactions in the near-surface at this study site is summarised in the cartoon shown in Fig. 10c. It is consistent with our interpretation of partitioned (extensional and contractional) ground deformation possibly driven by gravity gliding on destabilised gypsiferous marl - likely associated with salt withdrawal (Trude et al., 2012) or the collapse of salt pillars in the underground mines below the Keuper Marl (Arup et al., 1992) - and also the geochemical evolution of groundwater according to Chebotarev (1955) sequence. Our conceptual model posits that dissolution-induced fluid overpressure in clays ultimately causes gravitational gliding deformation (or landslides) in such environments. Obviously, our study is limited by the available 2D legacy data but a future detailed 3D acquisition of seismic and preferably controlled-source electromagnetic (audio-magnetotelluric) data can be used to test or refine our proposed mechanism of near-surface deformation as well as investigate the connections to deeper (up to 300 m deep) structures at this site that will be inaccessible to the conventional dc resistivity method.

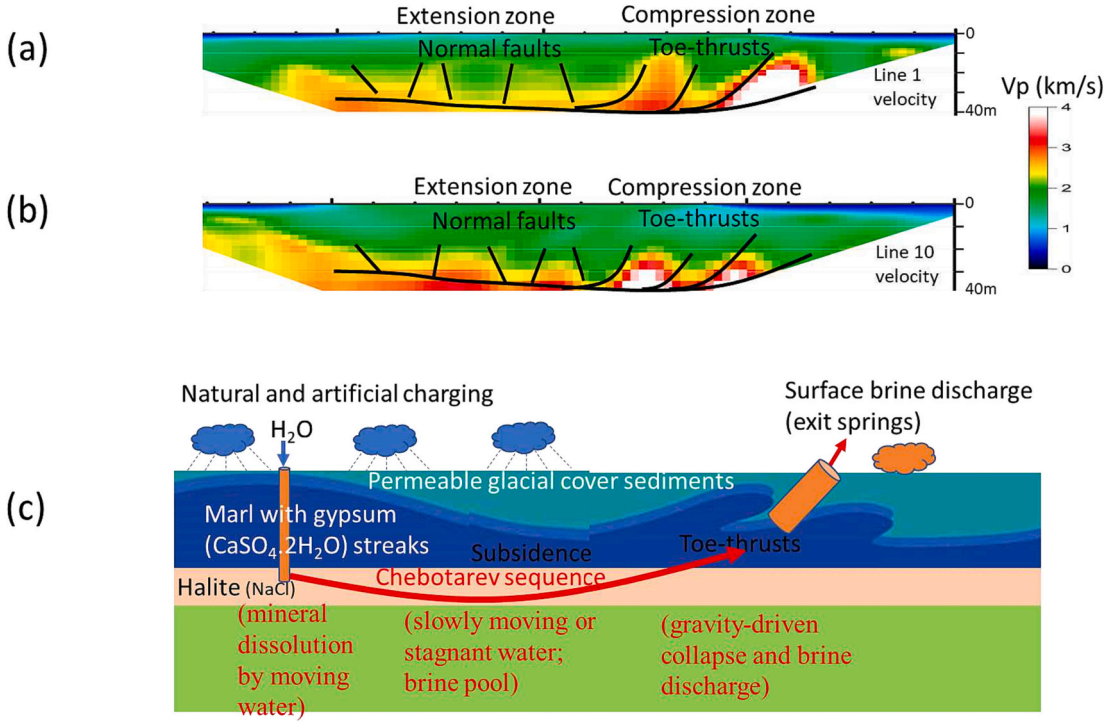

Fig. 10. Structural interpretation of the cross-gradient velocity models for line 1 (a) and line 10 (b) depicting possible extensional and contractual features typifying gravitational gliding systems. (c) Cartoon showing our conceptual model of water-rock-gravity interactions in the near-surface around the abandoned water-flooded salt mines in our study area. The proposed sequence of processes involved are water ingress, gypsum ($CaSO_4.2H_2O$) dissolution and enhanced permeability-fluid pressures in marl, marl weakening and detachment, mass transport by gravitational gliding (slumps, landslides) and exit springs (surface mud-brine flow).

5. Conclusion

Mine collapse and surface and subsurface contaminated discharges are two potential hazards that pose significant risks to urban areas, infrastructure, agriculture and heritage. Here, we use structurally-coupled cross-gradient inversion of seismic travel-time and electrical resistivity data combined with electrical self-potential (SP) data to characterise the upper 35 m of a former salt mining area in Carrickfergus, Northern Ireland, which is punctuated by a large upstream crown collapse. Our inverted cross-gradient data allow us to distinguish unsaturated from saturated till layers overlying the saturated gypsum-bearing marl member of the Triassic Mercia Mudstone Group. We were particularly able to delineate those glacial till and marl segments saturated with salt brine. Our SP data then confirm water ingress and salt brine seepage through the saturated till and marl layers down the hydraulic gradient into farmland and towards urban areas. Indeed, this seepage previously led to downstream surface spillage of salt brine contamination, which required remediation and therefore typifies the growing anthropogenic threat that such abandoned mines are posing. We can therefore conclude that state-of-the-science integrated geophysical imaging has the capacity to provide unique and spatially extensive information in support of identification and implementation of appropriate hazard mitigation measures at historic salt mines and their interconnections. Overall, we have shown that quantitative integration of Multiphysics data has the potential to maximize accuracy and reduce uncertainty in understanding the mechanism and processes underlying ground deformation and groundwater contamination in this former salt mining area. More importantly, they allowed us to determine the hitherto unknown gravity-driven deformation of the thick gypsum-bearing marl deposits and the geochemical zonation of groundwater in the area thus providing new understanding of the attendant deformation mechanism and processes in the near-surface which have implications for the future evolution of geohazards and their mitigation for such sites worldwide.

CRediT authorship contribution statement

Max A. Meju: Conceptualization, Formal analysis, Methodology, Resources, Software, Visualization, Writing – original draft, Writing – review & editing. **Bernd Kulessa:** Data curation, Formal analysis, Investigation, Methodology, Project administration, Supervision, Writing – original draft, Writing – review & editing. **Luis Gallardo:** Formal analysis, Methodology, Software, Visualization, Writing – review & editing. **Sarah Thompson:** Formal analysis, Methodology, Software, Visualization, Writing – review & editing. **Alastair Ruffell:** Formal analysis, Investigation, Methodology, Visualization, Writing – original draft, Writing – review & editing. **Kieran Parker:** Conceptualization, Methodology, Writing – review & editing.

Declaration of Competing Interest

The authors declare that they have no known competing financial interests or personal relationships that could have appeared to influence the work reported in this paper.

Data availability

Data will be made available on request.

Acknowledgment

We thank Gavin Hart and Richard Lennon for acquiring the geophysical data reported here as part of their student project. The critical comments from two anonymous reviewers are gratefully acknowledged.

Appendix A. Supplementary data

Supplementary data to this article can be found online at https://doi.org/10.1016/j.jappgeo.2023.105217.

References

Aghajani, H.F., 2018. The effect of embedded gypsum streaks on the dissolution of dam foundation: a case study in Iran. Sadhana 43 (5), 69.

Arup, O., et al., 1992. Report on the Site Investigation (Phase 2) of the Duncrue, Maiden Mount, Burleigh Hill and Black Pit salt mines at Carrickfergus, County Antrim, Northern Ireland, 43363/MIW/STJ/KWC.

Atkins, W.S. Ltd, 2005. Management of the abandoned salt mines at Carrickfergus, Co Antrim. In: Belfast: Report for the Department of Trade and Industry, Northern Ireland.

Bell, F.G., Donnelly, L.J., Genske, D.D., Ojeda, J., 2005. Unusual cases of mining subsidence from Great Britain, Germany and Colombia. Environ. Geol. 47 (5), 620–631.

Bolève, A., Janod, F., Mattiuzzo, J.L., Fry, J.-J., 2009. Preferential fluid flow pathways in embankment dams imaged by self-potential tomography. Near Surf. Geophys. 7, 447–462.

Carrier, A., Bottelin, P., Fabre, L., Mathy, A., 2022. Damage Assessment of supporting Pillars in an Underground Cave using Joint Inversion of Electrical Resistivity and P-wave Velocity, Burgundy (France). Pure Appl. Geophys. 179, 45–67.

Chebotarev, I.I., 1955. Metamorphism of natural waters in the crust of weathering. Geochim. Cosmochim. Acta 8, 198–212, 22-48, 137-170.

Cigna, F., Banks, V.J., Donald, A.W., Donohue, S., Graham, C., Hughes, D., McKinley, J. M., Parker, K., 2017. Mapping ground instability in areas of geotechnical infrastructure using satellite INSAR and small UAV surveying: a case study in Northern Ireland. Geosciences 7, 51. https://doi.org/10.3390/geosciences7030051.

Cooper, A.H., 2002. Halite karst geohazards (natural and man-made) in the United Kingdom. Environ. Geol. 42 (5), 505–512.

Cooper, A.H., 2020. Geological hazards from salt mining, brine extraction and natural salt dissolution in the UK. In: Giles, D.P., Griffiths, J.S. (Eds.), Geological Hazards in the UK: Their Occurrence, Monitoring and Mitigation- Engineering Group Working Party Report, The Geol. Soc. London, 29. Engineering Geology Special Publications, pp. 369–387.

Doetsch, J., Linde, N., Coscia, I., Greenhalgh, S.A., Green, A.G., 2010a. Zonation for 3D aquifer characterization based on joint inversions of multimethod crosshole geophysical data. Geophysics 75, G53–G64.

Doetsch, J., Linde, N., Binley, A., 2010b. Structural joint inversion of time-lapse crosshole ERT and GPR traveltime data. Geophys. Res. Lett. 37, L24404.

Doherty, R., Kulessa, B., Ferguson, A.S., Larkin, M.J., Kulakov, L.A., Kalin, R.M., 2010. A microbial fuel cell in contaminated ground delineated by electrical self-potential and normalized induced polarization data. Journal of Geophysical Research. Biogeosciences 115, G00G08.

Donald, A., 2015. New approaches to monitoring Northern Ireland's mining heritage. In: Presentation at GeoData2015, Stormont Hotel, Belfast, 5 November 2015.

Gallardo, L.A., Meju, M.A., 2003. Characterization of heterogeneous near-surface materials by joint 2D inversion of dc resistivity and seismic data. Geophys. Res. Lett. 30 (13), 1658.

Gallardo, L.A., Meju, M.A., 2004. Joint two-dimensional DC resistivity and seismic travel time inversion with cross-gradients constraints. J. Geophys. Res. Solid Earth 109 (B3), B03311.

Gallardo, L.A., Meju, M.A., 2011. Structure-coupled multiphysics imaging in geophysical sciences. Rev. Geophys. 49 (1), RG1003.

Gallardo, L.A., Fontes, S.L., Meju, M.A., Buonora, M.P., de Lugao, P., 2012. Robust geophysical integration through structure-coupled joint inversion and multispectral fusion of seismic reflection, magnetotelluric, magnetic and gravity images: example from Santos Basin, offshore Brazil. Geophysics 77 (5), B237–B251.

Griffith, A.E., Wilson, H.E., Bennett, J.R.P., 1983. Geology of the Country around Carrickfergus and Bangor: Sheet 29. Memoirs of the Geological Survey of Northern Ireland.

Hiemstra, J.F., Kulessa, B., King, E.C., Ntarlagiannis, D., 2011. The use of integrated sedimentological and geophysical methods in drumlin research – a case study of Pigeon Point, Clew Bay, Northwest Ireland. Earth Surf. Process. Landf. 36 (14), 1860–1871.

Knight, J., 2005. Formation of thrust structures in front of coastal landslides. J. Geol. 223, 107–114.

Krawczyk, C.M., Polom, U., 2018. Detection of mobile quick-clay layers using shear wave reflection seismics. In: Misra, A.A., Mukherjee, S. (Eds.), Atlas of Structural Geological Interpretation from Seismic Images, vol. 33, pp. 175–176.

Kulessa, B., Ruffell, A., Glynn, D., 2004. Characterising ground hazards induced by historic salt mining using ground-penetrating radar. In: de Fonseca, A.V., Mayne, P. W. (Eds.), Geotechnical and Geophysical Site Characterisation, volume 1. Millpress, Rotterdam.

Kulessa, B., Clarke, G., Hughes, D.A.B., Barbour, S.L., 2007. Anatomy and facies association of a drumlin in Co. Down, Northern Ireland, from seismic and electrical resistivity surveys. In: Hambrey, M.J., et al. (Eds.), Glacial Sedimentary Properties and Processes, Spec. Publ. Int. Assoc. Sediment, 39, pp. 165–176.

Mari, J.L., Arens, G., Chapellier, D., Guadiani, P., 1999. Geophysics of Reservoirs and Civil Engineering, Editions TECHNIP, 97–215. Institut Francais du Petrole publications, Paris, France, 456pp.

Meju, M.A., Gallardo, L.A., 2016. Structural coupling approaches in integrated geophysical imaging. In: Moorkamp, M., Lelièvre, P.G., Linde, N., Khan, A. (Eds.), Integrated Imaging of the Earth. Geophysical Monograph Series: American Geophysical Union, pp. 49–67.

Meju, M.A., Gallardo, L.A., Mohamed, A.K., 2003. Evidence for correlation of electrical resistivity and seismic velocity in heterogeneous near-surface materials. Geophys. Res. Lett. 30 (7), 1373.

Misra, A.A., 2018. Growth fault-thrust belts with single detachment in the Krishna–Godavari Basin, India. In: Misra, A.A., Mukherjee, S. (Eds.), Atlas of Structural Geological Interpretation from Seismic Images, Chap, vol. 34, pp. 177–182.

Moorkamp, M., Heincke, B., Jegen, M., Roberts, A.W., Hobbs, R.W., 2011. A framework for 3-D joint inversion of MT, gravity and seismic refraction data. Geophys. J. Int. 184, 477–493.

Moorkamp, M., Roberts, A.W., Jegen, M., Heincke, B., Hobbs, R.W., 2013. Verification of velocity-resistivity relationships derived from structural joint inversion with borehole data. Geophys. Res. Lett. 40 (14), 3596–3601.

Naudet, V., Revil, A., Rizzo, E., Bottero, J.Y., Bégassat, P., 2004. Groundwater redox conditions and conductivity in a contaminant plume from geoelectrical investigations. Hydrol. Earth Syst. Sci. 8 (1), 8–22.

Nicholson, C.A., 2014. Salt Mines in the Carrickfergus Area of County Antrim. J. Min. Herit. Trust of Ireland 14, 1–22.

Ordnance Survey map of Northern Ireland, 1930. Sheet 52, 1930, 1:10560, reproduced with Crown copyright permission 2019.

Petiau, G., 2000. Second Generation of Lead-lead Chloride Electrodes for Geophysical applications. Pure Appl. Geophys. 157 (3), 357–382.

Ruffell, A., Kulessa, B., 2009. Application of Geophysical Techniques in Identifying Illegally Buried Toxic Waste. Environmental Forensics 10, 196–207.

Sharma, P., 1997. Environmental and Engineering Geophysics. Cambridge University Press.

Thompson, S., Kulessa, B., Luckman, A., 2012. Integrated electrical resistivity tomography (ERT) and self-potential (SP) techniques for assessing hydrological processes within glacial lake moraine dams. J. Glaciol. 58 (211), 849–858.

Thompson, S.S., Kulessa, B., Benn, D.I., Mertes, J.R., 2017. Anatomy of terminal moraine segments and implied lake stability on Ngozumpa Glacier, Nepal, from electrical resistivity tomography (ERT). Sci. Rep. 7, 46766.

Trude, J., Graham, R., Pilcher, R., 2012. Salt-related structures on the Bristol Channel coast, Somerset (UK). In: Alsop, G.I., Archer, S.G., Hartley, A.J., Grant, N.T., Hodgkinson, R. (Eds.), 2012. Salt Tectonics, Sediments and Prospectivity, 363. Geol. Soc., London, Special Publications, pp. 533–544.

Um, E.S., Commer, M., Newman, G.A., 2014. A strategy for coupled 3D imaging of large-scale seismic and electromagnetic data sets: application to subsalt imaging. Geophysics 79 (3). ID1-ID13.